ACS APPLIED MATERIALS & INTERFACES

www.acsami.org

Research Article

Ultrasensitive Electrochemical Impedance Detection of *Mycoplasma agalactiae* DNA by Low-Cost and Disposable Au-Decorated NiO Nanowall Electrodes

Mario Urso,* Serena Tumino, Elena Bruno, Salvo Bordonaro, Donata Marletta, Guido Ruggero Loria, Adi Avni, Yosi Shacham-Diamand, Francesco Priolo, and Salvo Mirabella*

Cite This: https://dx.doi.org/10.1021/acsami.0c14679

Read Online

ACCESS | Metrics & More | Article Recommendations | Supporting Information

ABSTRACT: Nanostructured electrodes detecting bacteria or viruses through DNA hybridization represent a promising method, which may be useful in on-field applications where PCR-based methods are very expensive, time-consuming, and require trained personnel. Indeed, electrochemical sensors combine disposability, fast response, high sensitivity, and portability. Here, a low-cost and high-surface-area electrode, based on Au-decorated NiO nanowalls, demonstrates a highly sensitive PCR-free detection of a real sample of *Mycoplasma agalactiae* (Ma) DNA. NiO nanowalls, synthesized by aqueous methods, thermal annealing, and Au decoration, by electroless deposition, ensure a high-surface-area platform for successful immobilization of Ma thiolated probe DNA. The morphological, chemical, and electrochemical properties of the electrode were characterized, and a reproducible detection of synthetic Ma DNA was observed and investigated by impedance measurements. Electrochemical impedance spectroscopy (EIS) ascribed the origin of impedance signal to the Ma DNA hybridization with its probe immobilized onto the electrode. The electrode successfully discriminates between DNA extracted from healthy and infected sheep milk, showing the ability to detect Ma DNA in concentrations as low as 53 ± 2 copy number μL^{-1}. The Au-decorated NiO nanowall electrode represents a promising route toward PCR-free, disposable, rapid, and molecular detection.

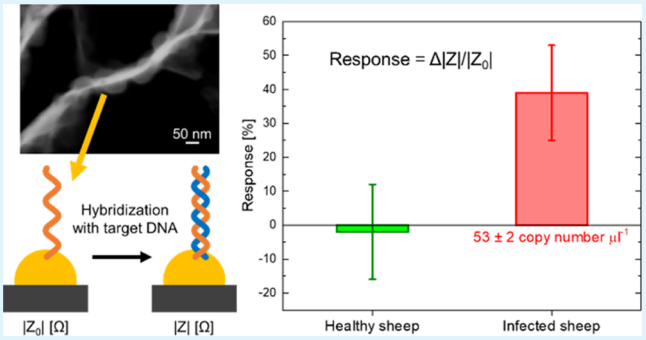

KEYWORDS: *label-free, PCR-free, DNA sensor, nickel oxide, gold nanoparticles, Mycoplasma agalactiae, contagious agalactia, electrochemical impedance spectroscopy*

1. INTRODUCTION

The coronavirus disease 2019 (COVID-19) outbreak showed once again how the lack of affordable, rapid, and accurate point-of-care (PoC) tests hinders the public health response to emerging viral and bacterial threats.[1,2] Viruses and bacteria responsible for diseases are typically identified after enrichment in specific media[3] and/or by highly sensitive and selective polymerase chain reaction (PCR)-based methods, where DNA is amplified before visualization.[4,5] However, the growth of microorganisms can be very slow,[6] while PCR is expensive, time-consuming, and requires laboratories with specialized staff due to its complex operational protocols.[7,8] Therefore, there is a pressing demand for low-cost, fast, and reliable PCR-free DNA sensors as tool for the specific identification of a wide range of microorganisms in different matrices.

DNA sensors are based on the detection of variations in the physical−chemical properties of a sensing element upon hybridization between an immobilized probe ssDNA and the complementary sequence. This approach ensures high selectivity because of the specificity of DNA base pairing.[9] Various strategies have been developed to detect DNA hybridization. As a result, a wide variety of DNA sensors have been reported, including optical, piezoelectric, and electrochemical transducers.[10]

Among the different devices developed so far, electrochemical sensors are very advantageous due to their robustness, miniaturization, sensitivity, and fast response along with low-cost/energy/mass characteristics and great potential as PoC devices intended for commercialization.[11,12] The working electrode is the core component of any electrochemical sensor, and for DNA sensors, it is where probe ssDNA is immobilized via physical absorption, self-assembly, or covalent bonds (as in the case of thiolated probe ssDNA and Au electrodes). Indeed,

Received: August 14, 2020
Accepted: October 9, 2020

the working electrode determines the ultimate properties of the sensor.[13,14] Upon hybridization of probe ssDNA with the complementary sequence, an electrochemical signal is generated whose amplitude defines the sensitivity of the sensor.[9] Various electrochemical techniques have been used to enhance the hybridization signal, including voltammetric, amperometric, coulometric, and impedimetric techniques.[15] Among them, electrochemical impedance spectroscopy (EIS) is considered a powerful technique to sensitively detect variations of the impedance of the electrode/electrolyte interface caused by DNA hybridization.[16−18] To measure the impedance, a very small-amplitude sinusoidal voltage is applied without interfering with the properties being measured.[19] The response can be evaluated from the impedance spectrum at different frequencies where its fitting with an equivalent circuit model is one option, or alternatively by following the impedance variations at a single frequency.[15]

To boost the sensitivity to DNA hybridization, much effort has been devoted to developing nanostructured electrodes with large surface area and porous structures, leading to a higher number of surface sites for the immobilization of probe ssDNA.[20,21] Still, there are issues with the cost and reproducibility of the fabrication processes of some nanostructured electrodes, as well as their stability.

Rapid detection of pathogens responsible for infectious diseases is still a major challenge for the scientific community. Among the different bacteria to detect, diagnosis of mycoplasmas such as *Mycoplasma agalactiae* (Ma) still represents a difficult task due to their peculiar metabolic requirements, slow and difficult growth in artificial media, and need of well-equipped laboratories for their identification. Ma is the principal etiological agent of contagious agalactia (CA) in sheep and goats, an infectious disease leading to a severe reduction and even suppression of milk production and, occasionally, to mortality.[22,23] Due to its morbidity, CA can rapidly spread in the whole flock, causing serious economic losses for farmers.[24] CA is found across several continents, including mainly North America, Western Asia, North Africa, and Europe, being endemic in most Mediterranean countries. Because of its large diffusion and important economic impact, the World Organization for Animal Health included CA in the list of notifiable diseases of animals.[25] Today, CA diagnosis is done by the observation of clinical signs, Ma culture in growth media, biochemical identification, and molecular detection methods as PCR-based methods and loop-mediated isothermal amplification assays (LAMP).[26−29]

Here, we report on the successful application of a novel nanostructured electrode for the PCR-free electrochemical detection of Ma DNA. The electrode is composed of Au-decorated NiO nanowalls grown by low-cost methods, on which a probe ssDNA specific of Ma was immobilized. A prehybridization step with a nonspecific ssDNA sequence was also performed to improve electrode stability and to prevent false positives from nonspecific interactions during sensing. The proposed electrode showed fast, sensitive, and selective response to Ma DNA, even at the very low concentration of 53 ± 2 copy number μL^{-1} extracted from infected sheep milk. The reported data demonstrate great potential for the PCR-free detection of Ma DNA, which in principle can be applied to detect other similar DNA sequences, including viral ones.

2. EXPERIMENTAL SECTION

2.1. Synthesis of NiO Nanowalls. Conductive substrates (1 × 2 cm^2), consisting of an ∼50 nm thick Au layer on an ∼15 nm thick Ti adhesion layer deposited by evaporation onto an ∼100 nm thick SiO_2 layer on c-Si substrates (cut from Czochralski wafers) or Ni foam substrates (1 × 2 cm^2, Goodfellow; thickness, 1.6 mm; porosity, 95%; 20 pores cm^{-1}) were rinsed with acetone, isopropanol, and deionized water (Milli-Q, 18 MΩ cm) and dried under N_2 gas flow. $Ni(OH)_2$ nanowalls were grown on cleaned substrates by low-cost chemical bath deposition (CBD).[30] The CBD solution consisted of 0.42 M $NiSO_4 \cdot 6H_2O$ (Alfa Aesar, 98%), 0.07 M $K_2S_2O_8$ (Alfa Aesar, 97%), and 3.5 wt % NH_3 (Merck, 30−33 v/v%) in deionized water. The solution was heated up to 50 °C. The substrates were immersed (1 × 1.5 cm^2) for 20 min, then rinsed with deionized water to remove unwanted microparticulate, and dried under N_2 gas flow. The as-deposited $Ni(OH)_2$ nanowall samples were further annealed at 350 °C for 1 h in an inert atmosphere to obtain NiO nanowalls.[31,32]

2.2. Decoration with Au Nanoparticles. NiO nanowalls were decorated with Au by low-cost electroless deposition (ELD), following the procedure of Vorobyova et al.[33] Prior to ELD, NiO nanowalls were immersed for 10 min in 7.5 v/v% $N_2H_4 \cdot H_2O$ (Sigma-Aldrich, 50−60 v/v%) at room temperature for surface activation and rinsed with deionized water. The ELD solution consisted of 2 g L^{-1} $KAu(CN)_2$ (Sigma-Aldrich, 98%), 45 g L^{-1} $Na_3C_6H_5O_7 \cdot 2H_2O$ (Sigma-Aldrich), 70 g L^{-1} NH_4Cl (Sigma-Aldrich, ≥99.5%), and 8 g L^{-1} $NaH_2PO_2 \cdot H_2O$ (Merck, ≥99%) in deionized water. The pH of the solution was adjusted to 7.5, and the solution was heated up to 80−85 °C. NiO nanowall samples were immersed for 3 min in the solution to obtain Au-decorated NiO nanowalls, then rinsed with deionized water, and dried under N_2 gas flow.

2.3. Immobilization of Probe DNA. *M. agalactiae* (Ma) synthetic probe ssDNA (probe DNA) had the 28-base sequence with a thiol on 5′ end HS-C6-TGT GAT GAT AAG AAC GAA AAT TCA CAA A (Hylabs, 8990 Da molecular weight), eventually modified with a cyanine (Cy3) on 3′ end (Hylabs, 9577 Da molecular weight). This peculiar DNA sequence, based on *p40* target gene, encoding an immunodominant adhesin that has a central role in mycoplasma adhesion and virulence, was chosen since it ensures selectivity to the Ma with respect to other mycoplasmas.[26] Thiolated DNA was used to achieve robust binding on the Au nanoparticles surface.[11,34,35] The solution for immobilization consisted of 1X TE buffer, i.e., 10 mM Tris ($C_4H_{11}NO_3$, Sigma-Aldrich, ≥99.8%), 1 mM EDTA ($C_{10}H_{16}N_2O_8$, Sigma-Aldrich, ≥99%), 40 mM NaCl (Sigma-Aldrich, ≥99.5%), 5 mM $MgCl_2$ (Sigma-Aldrich, ≥98%), 4.5 μM probe DNA, and 0.5 μM Cy3-modified probe DNA in deionized water. Au-decorated NiO nanowalls were immersed in the solution for 5 h at room temperature under stirring (100 rpm), then rinsed with deionized water, and dried under N_2 gas flow.

2.4. Prehybridization with Nonspecific DNA. Synthetic noncomplementary ssDNA (nonspecific ssDNA) for prehybridization had the 30-base sequence ATG GTC TCA CTG CTC TGC ACC AGC GGG GAA (Hylabs, 9168 Da molecular weight). The solution for prehybridization consisted of 2.5 mL of 0.1 M PBS (Sigma-Aldrich) (pH 7) at 40 °C and 12 μM nonspecific ssDNA. Au-decorated NiO nanowalls with probe DNA were immersed in the solution for different durations, from 1 to 5 h, and then rinsed with deionized water and dried under N_2 gas flow.

2.5. Test with Synthetic Target DNA. Ma synthetic complementary ssDNA (target DNA) for hybridization had the 28-base sequence TTT GTG AAT TTT CGT TCT TAT CAT CAC A (Hylabs, 8510 Da molecular weight). The solution for hybridization consisted of 2.5 mL of 0.1 M PBS (pH 7) at 40 °C with different concentrations (0.2, 1 and 1.5 μM) of target DNA. After 5 h prehybridization, Au-decorated NiO nanowalls with probe DNA were immersed in the solution for 1 h, then rinsed with deionized water, and dried under N_2 gas flow. Then, electrochemical measurements were conducted to detect impedance variation due to the hybridization with target DNA. It is worth noting that the dsDNA obtained upon hybridization was denatured only after the last electrochemical

https://dx.doi.org/10.1021/acsami.0c14679
ACS Appl. Mater. Interfaces XXXX, XXX, XXX−XXX

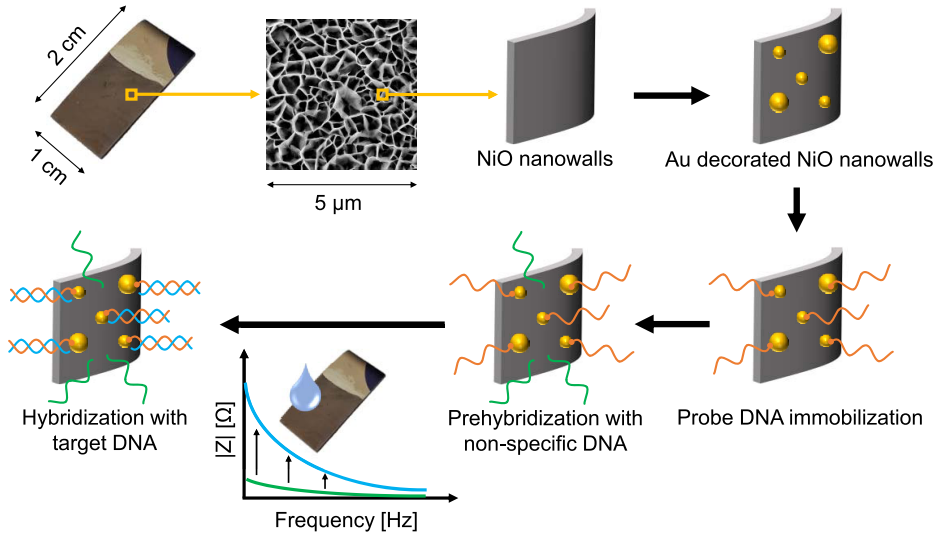

Figure 1. Schematic diagram of the DNA sensor based on Au-decorated NiO nanowalls from electrode fabrication to *M. agalactiae* DNA detection by measuring the variation of electrode impedance upon hybridization.

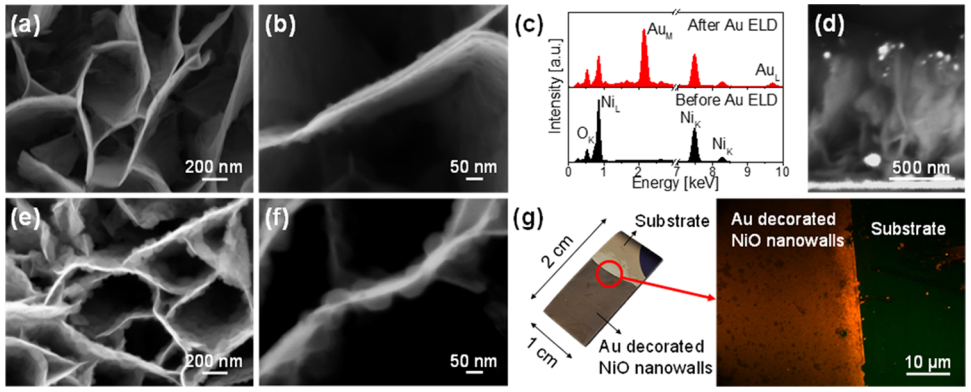

Figure 2. (a, b) Plan-view SEM images at different magnifications of NiO nanowalls. (c) EDX spectra of NiO nanowalls before (black) and after (red) Au decoration by ELD. (d) Cross-view SEM image acquired in backscattering mode of Au-decorated NiO nanowalls. (e, f) Plan-view SEM images at different magnifications of Au-decorated NiO nanowalls after probe DNA immobilization. (g) Photo of the electrode and plan-view micrograph acquired by a confocal microscope (~510 nm excitation wavelength) of Au-decorated NiO nanowalls after probe DNA immobilization.

experiment with synthetic target DNA by immersion in 1 M NaOH at 90−95 °C, followed by a new prehybridization for 5 h.

2.6. DNA Extraction from Milk Samples and Test. A milk sample was collected from a sheep with clear symptoms of CA, affected by interstitial mastitis, and alteration in the consistency of the milk with decline of milk production. The presence of Ma in the milk sample was confirmed by microbiological identification and real-time PCR at the OIE Reference Laboratory for Contagious agalactia at the Istituto Zooprofilattico Sperimentale della Sicilia according to the World Organization for Animal Health. A milk sample was also collected from a sheep previously checked to be Ma-free.

The genomic DNA was extracted from 1 mL of milk of infected and healthy sheep, using a Chelex-based InstaGene Matrix (Bio-Rad Laboratories, Hercules, CA) according to the manufacturer's instructions. The cell lysis phase occurs by boiling in the presence of InstaGene matrix, which absorbs the cell lysis products. Briefly, 1 mL of the milk sample was centrifuged at 12 000 rpm for 3 min, the supernatant was removed, and after addition of InstaGene Matrix, the suspension was incubated at 56 °C for 25−30 min, followed by heating at 100 °C for 12 min. After final centrifugation at 13 000 rpm for 3 min, the supernatant containing the extracted DNA was collected and stored at −20 °C.

Real-time PCR was used to measure the amount of Ma DNA in 2 μL of DNA from infected sheep milk through the comparison with a standard sample, which was tested in serial 10-fold dilution, i.e., 109 bp of p40 gene in a concentration ranging from 2 to 200 000 copies (each concentration was tested in duplicate).

Prior to hybridization, DNA obtained from infected and healthy sheep were heated up to 90−95 °C to denature the DNA. Then, hybridization with target DNA from milk samples was achieved by immersion in a 2.5 mL solution at 40 °C, made by diluting 20 μL of the milk sample in 2480 μL of 0.1 M PBS (pH 7).

2.7. Characterization. The surface morphology of samples was characterized by a scanning electron microscope (Gemini field emission SEM Carl Zeiss SUPRA 25) combined with energy-dispersive X-ray spectroscopy (EDX). It is worth noting that EDX analyses were carried out on samples grown on Ni foam substrates. SEM images in backscattering mode were acquired using a Versa 3D DualBeam (FIB/SEM). Cy3 fluorescence was observed by a confocal microscope with an excitation wavelength of ~510 nm.

Electrochemical impedance spectroscopy (EIS) measurements were performed using a BioLogic VSP and VersaSTAT 4 potentiostats. All measurements were performed in a three-electrode setup with a Pt wire as the counter electrode, a commercial silver/silver chloride electrode (Ag/AgCl, 1 M KCl internal solution) as the reference electrode, and samples as working electrodes (1 × 1 cm^2 active area). All measurements were performed at room temperature in a 0.1 M PBS solution at pH 7 as the supporting electrolyte, containing 10 mM $[Fe(CN)_6]^{3-/4-}$ (Sigma-Aldrich, ≥99%) as redox probe, at 0 V vs open-circuit potential with 10 mV superimposed

https://dx.doi.org/10.1021/acsami.0c14679
ACS Appl. Mater. Interfaces XXXX, XXX, XXX−XXX

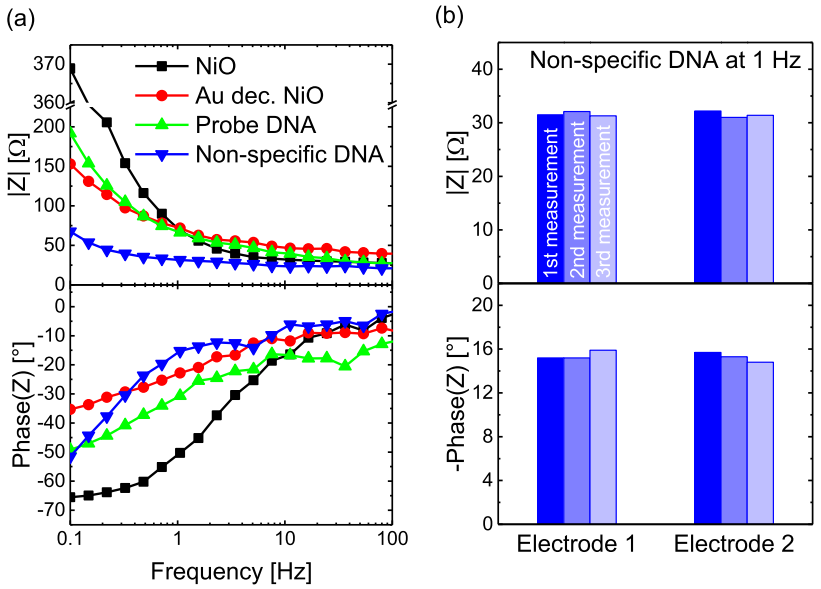

Figure 3. (a) |Z| and *Phase(Z)* as a function of the frequency of NiO nanowalls (black squares), Au-decorated NiO nanowalls (red circles), probe DNA immobilization (green up triangles), and 5 h prehybridization with nonspecific DNA (blue down triangles), as obtained by EIS measurements. (b) |Z| and *Phase(Z)* at 1 Hz for three EIS measurements of two electrodes after 5 h prehybridization with nonspecific DNA.

sinusoidal voltage in the frequency range of 100−0.1 Hz. EIS measurements were repeated at least three times at each step for two electrodes prepared under similar conditions.

3. RESULTS AND DISCUSSION

3.1. Electrode Fabrication. Figure 1 shows the schematic diagram of the novel DNA sensor based on Au-decorated NiO nanowalls, reporting all of the steps from electrode fabrication to *M. agalactiae* (Ma) DNA detection. NiO nanowalls were grown on conductive substrates by low-cost chemical bath deposition (CBD) and low-temperature thermal annealing in inert atmosphere and served as a high-surface-area platform for further decoration with Au nanoparticles by a low-cost electroless deposition (ELD). Ma thiolated probe ssDNA (probe DNA) was immobilized onto Au-decorated NiO nanowalls using the strong covalent bond between S in thiol and Au. Then, a prehybridization step with nonspecific DNA was performed to saturate further adsorption sites, if any, and to obtain a stable electrochemical behavior. After hybridization with Ma complementary ssDNA (target DNA), the response of the sensor was evaluated as the variation of electrode impedance by electrochemical impedance spectroscopy (EIS) measurements using the usual three-electrode configuration and 0.1 M PBS (pH 7) with $[Fe(CN)_6]^{3-/4-}$ as a redox probe.

Scanning electron microscopy (SEM) analyses after each step of electrode fabrication revealed the surface morphology. The plan-view SEM images at different magnifications in Figure 2a,b show the characteristic morphology of bare NiO nanowalls: a porous and nanostructured film formed by a tight network of interconnected nanosheets with lateral thickness of ∼20 nm and height of ∼1 μm, resulting in a surface enhancement by a factor of 16 ± 2, as estimated from SEM images analysis.

A chemical analysis by energy-dispersive X-ray spectrometry (EDX) performed before and after Au ELD on NiO nanowalls assessed the presence of Au. The obtained spectra are compared in Figure 2c. Ni and O peaks due to the NiO nanowalls are obviously present in both spectra. However, the spectrum of NiO nanowalls after Au ELD displays also the distinctive peaks of Au_M and Au_L transitions, suggesting a successful decoration with Au. Figure 2d reports a cross-view SEM image of Au-decorated NiO nanowalls acquired in backscattering mode to enhance the contrast between Au and Ni, showing the ∼1 μm high nanowalls decorated with Au nanoparticles on top, mainly. A large density of Au nanoparticles with radius ≤30 nm is observed onto the nanowalls. A few bigger Au nanoparticles (∼50 nm) are observed in the inner regions, as a result of the porous nature of the film.

The successful decoration of NiO nanowalls with Au nanoparticle can be appreciated also in Figure 2e,f, where samples after probe DNA immobilization are presented. The comparison with Figure 2a,b allows us to see how the NiO nanowalls show the same morphology (as expected) but gently covered by hemispherical particles (20−50 nm in diameter) on both sides. Assuming a base pair length of approximately 3.4 Å,[36] the size of the hemispherical particles is consistent with that expected from an ∼9.5 nm long 28-base DNA sequence immobilized onto 30-nm-sized Au nanoparticles. The observed larger size of nanostructures after DNA immobilization agrees with the literature reporting an increase of size and surface roughness of nanostructures after DNA immobilization.[19,37] Since a fraction of the immobilized probe DNA had the Cy3 fluorescent dye at one end, the fluorescence was checked using a confocal microscope to further demonstrate the successful DNA immobilization onto the Au-decorated NiO nanowalls. Figure 2g reports the plan-view micrograph of the region straddling between substrate and Au-decorated NiO nanowalls, as indicated in the photo of the sensor electrode. A bright and uniform fluorescence is observed from Au-decorated NiO nanowalls as a result of a massive immobilization of probe DNA.

Electrochemical impedance spectroscopy (EIS) was used to investigate the electrode behavior after each step of fabrication. All tests were performed on two independently prepared electrodes, to have a coarse asset of the electrode reproducibility. EIS measurements were repeated three times

https://dx.doi.org/10.1021/acsami.0c14679
ACS Appl. Mater. Interfaces XXXX, XXX, XXX−XXX

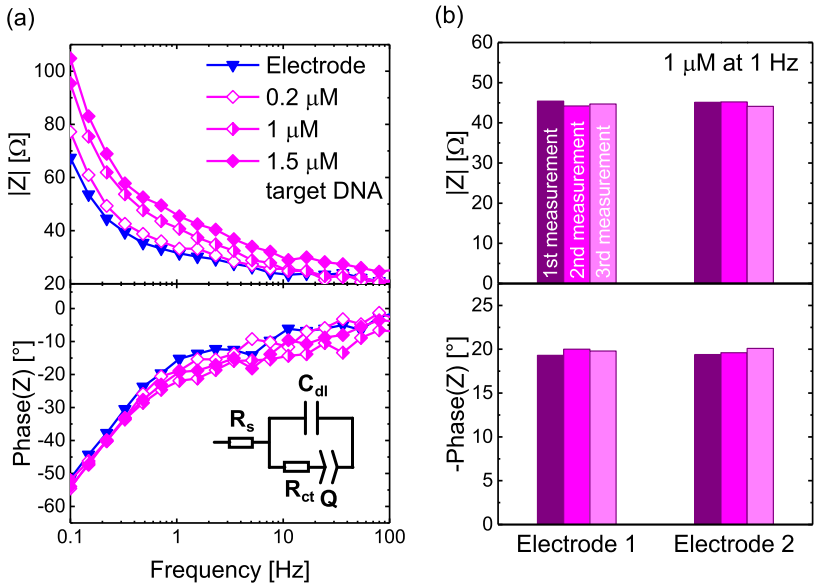

Figure 4. (a) |Z| and *Phase(Z)* as a function of the frequency of the electrode after fabrication (blue down triangles) and hybridization with different concentrations of synthetic target DNA (0.2 μM magenta open diamonds, 1 μM magenta half diamonds and 1.5 μM magenta diamonds), as obtained by EIS measurements (the inset is the equivalent circuit model). (b) |Z| and *Phase(Z)* at 1 Hz for three EIS measurements of two electrodes after hybridization with 1 μM synthetic target DNA.

Table 1. Circuit Parameters Obtained by Fitting EIS Data through the Equivalent Circuit Model Reported in Figure 4a

	R_{ct} [Ω]	C_{dl} [mF]	Q [mF s^{n-1}]	n	R_{sol} [Ω]
electrode	10.9 ± 0.9	4.0 ± 0.4	24 ± 1	0.85 ± 0.02	22.3 ± 0.4
0.2 μM	12 ± 2	3.7 ± 0.6	20 ± 1	0.86 ± 0.04	23.7 ± 0.7
1 μM	18 ± 2	1.5 ± 0.5	17 ± 2	0.8 ± 0.05	21 ± 1
1.5 μM	19 ± 2	1.5 ± 0.5	16 ± 1	0.82 ± 0.05	26 ± 1

for each electrode. Figure 3a shows the typical frequency-dependent impedance Z (|Z| and *Phase(Z)* vs frequency), recorded for NiO nanowalls (NiO), Au-decorated NiO nanowalls (Au dec. NiO), probe DNA immobilization (probe DNA), and 5 h prehybridization with nonspecific DNA (nonspecific DNA) (the corresponding Nyquist plots showing the real vs imaginary part of the impedance are reported in Figure S4). There is no significant change in |Z| from 100 000 to 3−4 Hz (100 000−100 Hz not shown here), while in the low-frequency region, large differences appear. The |Z| shows a marked increase for frequency decrease, and at 0.1 Hz, the largest differences between the samples are observed. After decoration with Au nanoparticles, in the low-frequency region, |Z| decreases as a result of a Schottky junction between Au (metal) and NiO (semiconductor) where Au acts as an electron acceptor, leaving a larger number of holes in *p*-type NiO.[38] |Z| slightly increases after probe DNA immobilization and decreases after prehybridization with nonspecific DNA due to the modification of the charge transfer and capacitive properties of the electrode/electrolyte interface. *Phase(Z)* shows a more complex dependency from frequency than |Z|. Still, the largest differences are observed in the low-frequency region where an intermediate behavior between a resistor (0°) and a capacitor (−90°) is noted. During the last step of electrode fabrication, a prehybridization with nonspecific DNA is performed and its duration is tested from 1 to 5 h (Figure S2). Both |Z| and *Phase(Z)* decrease until they stabilize, so we chose 5 h of prehybridization as the most effective prehybridization time. Figure 3b reports |Z| and *Phase(Z)* measured at 1 Hz for the two independently prepared electrodes. Both show similar values for |Z| (∼30 Ω) and −*Phase(Z)* (∼15°) after three consecutive measurements. The same trend is observed also at other frequencies, such as 0.1, 0.3, and 3 Hz (Figure S3). The variation in |Z| and *Phase(Z)* is below 3%, demonstrating the excellent reproducibility of the proposed fabrication route and the high electrochemical stability of the electrodes over time.

3.2. DNA Detection. To assess the expected impedance variations due to hybridization with target DNA from sheep milk samples, EIS was carried out after hybridization with high concentrations of synthetic target DNA ranging from 0.2 to 1.5 μM. Figure 4a shows the typical plots for |Z| and *Phase(Z)* vs frequency recorded before and after hybridization (the corresponding Nyquist plots are reported in Figure S4). The common behavior is that as the frequency decreases, both |Z| and *Phase(Z)* increase at a fixed DNA concentration, as already observed. However, at increasing concentrations of target DNA, |Z| increases while *Phase(Z)* does not change significantly, especially in the low-frequency region. It is worth noting that |Z| and *Phase(Z)* measured three times at 1 Hz for the two independently prepared electrodes after hybridization with 1 μM (Figure 4b), as well as for other target DNA concentrations, are similar. Specifically, the variation in |Z| and *Phase(Z)* is below 2%, confirming the high reproducibility and stability of the electrode and DNA detection.

EIS data fitting through an appropriate equivalent circuit model provides more information about the processes occurring at the electrode/electrolyte interface. |Z| and *Phase(Z)* vs frequency data of the electrode before and after

https://dx.doi.org/10.1021/acsami.0c14679
ACS Appl. Mater. Interfaces XXXX, XXX, XXX−XXX

hybridization with synthetic target DNA at various concentrations were well-fitted using the circuit reported in the inset in Figure 4a. This simple circuit consists of solution resistance (R_{sol}), double-layer capacitance (C_{dl}) formed by ions in proximity of the electrode, charge transfer resistance (R_{ct}), which takes into account the current flow due to redox reactions at the electrode/electrolyte interface, and a constant phase element (Q), with n being an ideality factor ($n = 1$ for an ideal capacitor). The obtained fits are shown in Figure S5, while the values obtained for circuit parameters are reported in Table 1.

From Table 1, it can be noted that all fit parameters show large variations up to 1 μM, while above this target DNA concentration, they roughly saturate. The observed saturation suggests that all immobilized probe DNA sequences have undergone hybridization with target DNA. Among the different circuit elements, C_{dl} and R_{ct} show the largest variation, from 4 to 1.5 mF, the former, and from 10.9 to 19 Ω, the latter. These changes elucidate the |Z| dependence observed in Figure 4a. In fact, for a capacitor, it is $|Z| = 1/\omega C$, where ω is the frequency and C is the capacitance, and for a resistor, it is $|Z| = R$, where R is the resistance. Thus, the variations in C_{dl} and R_{ct} are consistent with the |Z| increase at a fixed frequency in Figure 4a.

The increase of R_{ct} with target DNA concentration can be attributed to:

- the higher density of nonconductive DNA on electrode surface[5,39] and[5,39]
- the larger Coulomb repulsion between the redox probe ($[Fe(CN)_6]^{3-/4-}$) and the higher density of DNA phosphate groups (PO_4^{3-}) on electrode surface.[16,40,41]

The decrease of C_{dl} with target DNA concentration can be related to:

- the hindered faradic redox processes[42] and[42]
- the lower dielectric constant of biomolecules like DNA with respect to a water-based electrolyte (≈2−5 vs 80).[15]

On the basis of the proposed mechanism, the response to target DNA can be evaluated as the variation of R_{ct} or C_{dl} to the target DNA concentration. However, this approach is more difficult and time-consuming than monitoring |Z| at a fixed frequency, since it would employ the impedance measurement on a relatively wide frequency range and data fitting. Therefore, the response to target DNA was defined as the |Z| variation at a fixed frequency

$$\text{response} = \frac{|Z_{\text{target DNA}}| - |Z_{\text{non-specific DNA}}|}{|Z_{\text{non-specific DNA}}|} \times 100$$

where $|Z_{\text{target DNA}}|$ and $|Z_{\text{non-specific DNA}}|$ are the moduli of the impedance (measured at a single frequency) after prehybridization with nonspecific DNA and hybridization with target DNA, respectively. Since the responses to a fixed target DNA concentration calculated at 1, 0.3, and 0.1 Hz were almost equal (Figure S6), only the response at 1 Hz was considered for further investigations with real DNA samples, as lower frequencies can induce higher noise out of laboratories.

To validate the on-field applicability of the proposed electrode for Ma DNA detection, we extracted the DNA from the milk of healthy and infected sheep. Real-time PCR was used to evaluate the amount of Ma DNA in the milk of the infected sheep through the comparison with a standard sample by testing serial 10-fold dilution of plasmid containing 109 bp of p40 gene in a concentration ranging from 2 to 200 000 copies (each dilution was tested in duplicate).[43] Figure 5a shows the linear regression curve, i.e., cycle threshold (Ct) vs logarithm of copy number of the standard sample (black squares). Based on this calibration, the Ma DNA in 2 μL sheep milk (red circle in Figure 5a) was estimated to be 13 335 ± 440 copy number, that is, 6668 ± 440 copy number μL^{-1}. For hybridization experiment, 20 μL of the DNA extracted from infected sheep milk was diluted in 0.1 M PBS up to a final volume of 2.5 mL; thus, the Ma DNA concentration experienced by the electrode is 53 ± 2 copy number μL^{-1}.

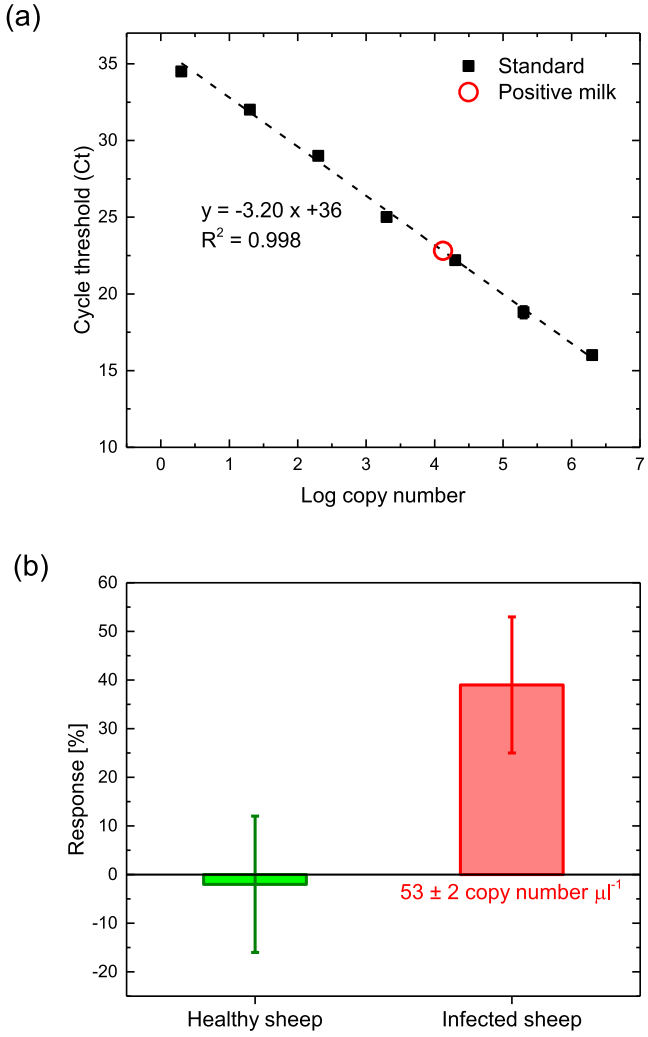

Figure 5. (a) Linear regression curve of the Ma real-time PCR assay generated using 10-fold serial dilutions of standard Ma DNA and the corresponding cycle threshold (Ct) values (black squares), and DNA extracted from infected sheep milk (red circle). Each dilution was tested in duplicate, and the error bars are of the same size as the symbols. (b) Electrode response to DNA extracted from healthy (green column) and infected sheep milk (red column).

The response to DNA extracted from healthy and infected sheep milk was tested by measuring the variation of |Z| at 1 Hz (Figure 5b). The test with DNA extracted from healthy sheep milk gave a null response (green column in Figure 5b) as it does not contain Ma DNA, but rather the ovine DNA and, potentially, other microorganisms in milk. A slightly negative

https://dx.doi.org/10.1021/acsami.0c14679
ACS Appl. Mater. Interfaces XXXX, XXX, XXX−XXX

response is consistent with the |Z| decrease observed during prehybridization with nonspecific DNA (Figure S2). This result indicates that our electrode is essentially not affected by immersion in the milk DNA solution.

The test with DNA extracted from infected sheep milk was successful (red column in Figure 5b); in fact, it gave a positive response (~40%), proving that DNA hybridization is very effective despite the natural Ma DNA is much longer than the synthetic one. Moreover, it demonstrates the great potential of the electrode, as it is capable of detecting Ma DNA in the concentration of 53 copy number μL^{-1}, almost approaching the minimum amount of 20 copy number per reaction measured by our real-time PCR analysis, which is similar to those reported in other studies.[26,43,44]

The reported results suggest that our electrode based on Au-decorated NiO nanowalls can undoubtedly distinguish between healthy and infected sheep by looking for |Z| variations induced by Ma DNA in milk samples. The sensor is extremely selective due to the intrinsic selectivity of DNA hybridization,[9] and to the prehybridization step with nonspecific DNA, which lowers the probability of getting false positives from nonspecific interactions with other molecules in milk samples. Our sensor fabrication route is simple, cheap, and reproducible. Moreover, solutions for sensor fabrication and DNA detection can be directly spotted onto miniaturized screen-printed electrodes, which add many advantages such as low amount of active material, low sample volume to be examined, and portability.[45] Based on this, our sensor can be used in disposable mode for on-field analysis. Apart from the DNA extraction from milk samples, the simple sensor operation does not require specialized staff. Thereby, it represents a powerful tool to quickly identify infected sheep and isolate them to limit Ma diffusion in the whole flock and avoid major economic losses for farmers.

The obtained response is satisfactory, and it can be further improved by increasing the amount of immobilized probe DNA.[46] This requires a higher density of Au nanoparticles on NiO nanowalls after electroless decoration step. Still, one major drawback of the proposed sensor is the relatively long hybridization time (1 h) compared to the short response time of a few seconds. The hybridization time can be lowered by optimizing the hybridization temperature and the salinity of the hybridization solution. These considerations are the basis for future works. Nevertheless, the proposed electrode represents an unprecedented demonstration of Ma DNA detection through a simple electrode and without any amplification-based method. It is worthy to note that our electrode can be used to detect, in principle, any DNA employing the proper immobilization of the relative probe DNA on Au-decorated NiO nanowalls.

4. CONCLUSIONS

In this work, a low-cost and high-surface-area electrode, based on Au-decorated NiO nanowalls, shows an unprecedented, PCR-free detection of a bacterium ssDNA. The electrode presents a large exposed sensing area thanks to the chemical bath-deposited NiO nanowalls, offering a tight network of substrate-perpendicular and interconnected nanosheets (~20 nm thick, 1 μm tall). The careful decoration with Au nanoparticles (radius ≤30 nm), by electroless deposition, serves for successful immobilization of *M. agalactiae* (Ma) thiolated probe ssDNA. A prehybridization step with a nonspecific DNA sequence allows us to saturate the electrode surface, leading to a stable electrochemical behavior and a lower probability of getting false positives from nonspecific interactions during sensing experiments. The electrode responds to high concentrations of synthetic target ssDNA (0.2−1.5 μM), as measured by the variation of electrode impedance at a fixed frequency. EIS clarifies that such variations are attributed to the increase of the charge transfer resistance and decrease of the capacitance at the electrode/electrolyte interface with a higher concentration of DNA. Moreover, the electrode successfully reacts with DNA extracted from infected sheep milk and is unresponsive to DNA from infected sheep milk. The response to DNA extracted from infected sheep milk at a concentration as low as 53 ± 2 copy number μL^{-1} and the absence of response to DNA from healthy sheep milk demonstrate the great potential of the proposed electrode for low-cost, rapid, on-field, and PCR-free Ma DNA detection. Our electrode based on Au-decorated NiO nanowalls is suitable for a fast, selective, and high-sensitivity detection of other viruses or bacteria, after immobilization of the probe ssDNA sequence on the Au nanoparticles.

■ ASSOCIATED CONTENT

Supporting Information

The Supporting Information is available free of charge at https://pubs.acs.org/doi/10.1021/acsami.0c14679.

Nyquist plots at different stages of electrode fabrication (Figure S1), impedance modulus and phase vs frequency for different prehybridization times with nonspecific DNA (Figure S2), electrode reproducibility and stability after prehybridization with nonspecific DNA at various frequencies (Figure S3), Nyquist plots (Figure S4), fits of impedance modulus and phase (Figure S5), and response at various frequencies to several concentrations of synthetic target DNA (Figure S6) (PDF)

■ AUTHOR INFORMATION

Corresponding Authors

Mario Urso − *Dipartimento di Fisica e Astronomia "Ettore Majorana", Università di Catania, and IMM-CNR, 95123 Catania, Italy*; orcid.org/0000-0001-7993-8138; Email: mario.urso@dfa.unict.it

Salvo Mirabella − *Dipartimento di Fisica e Astronomia "Ettore Majorana", Università di Catania, and IMM-CNR, 95123 Catania, Italy*; Email: salvo.mirabella@dfa.unict.it

Authors

Serena Tumino − *Dipartimento di Agricoltura, Alimentazione e Ambiente, Università di Catania, 95123 Catania, Italy; OIE Reference Laboratory for Contagious Agalactia—Istituto Zooprofilattico Sperimentale della Sicilia, 90129 Palermo, Italy*

Elena Bruno − *Dipartimento di Fisica e Astronomia "Ettore Majorana", Università di Catania, and IMM-CNR, 95123 Catania, Italy*

Salvo Bordonaro − *Dipartimento di Agricoltura, Alimentazione e Ambiente, Università di Catania, 95123 Catania, Italy*

Donata Marletta − *Dipartimento di Agricoltura, Alimentazione e Ambiente, Università di Catania, 95123 Catania, Italy*

Guido Ruggero Loria − *OIE Reference Laboratory for Contagious Agalactia—Istituto Zooprofilattico Sperimentale della Sicilia, 90129 Palermo, Italy*

https://dx.doi.org/10.1021/acsami.0c14679
ACS Appl. Mater. Interfaces XXXX, XXX, XXX−XXX

Adi Avni − *School of Plant Sciences and Food Security, Tel Aviv University, Tel-Aviv 69978, Israel*

Yosi Shacham-Diamand − *Department of Physical Electronics, School of Electrical Engineering and Department of Materials Science and Engineering, Faculty of Engineering, Tel Aviv University, Tel-Aviv 69978, Israel; TAU/TiET Food Security Centre of Excellence (T2FSCOE), Thapar Institute of Engineering and Technology, Patiala 147004, Punjab, India*

Francesco Priolo − *Dipartimento di Fisica e Astronomia "Ettore Majorana", Università di Catania, and IMM-CNR, 95123 Catania, Italy*

Complete contact information is available at: https://pubs.acs.org/10.1021/acsami.0c14679

Author Contributions

M.U. fabricated the nanostructured electrode, acquired and analyzed the data, generated the figures, and drafted the manuscript; E.B. performed SEM analysis; S.T., S.B., D.M., and G.R.L. supplied the Ma DNA sheep milk, performed PCR analysis, and contributed to data analysis; F.P., A.A., Y.S.-D., and S.M. conceived the idea, contributed to data analysis and interpretation, and supervised the project. All authors commented and reviewed the manuscript at all stages.

Funding

This work was supported by PON MIUR ADAS+ (ARS01_00459) and "Materiali innovativi e nanostrutturati per microelettronica, energia e sensoristica"—Linea di intervento 2 (Univ. Catania, DFA).

Notes

The authors declare no competing financial interest.

■ ACKNOWLEDGMENTS

The authors would like to thank Dr. Alexandra Inberg and Dr. Yelena Sverdlov (Department of Physical Electronics, Tel Aviv University) for their advice and assistance on Au electroless deposition, Dr. Christian Heck and Prof. Yuval Ebenstein (Department of Chemical Physics, Tel Aviv University) for their advice and assistance on probe DNA immobilization, and Mr. Luca Bruno (Dipartimento di Fisica e Astronomia, Università di Catania) for the preparation of samples for EDX analysis. The authors thank also Bio-nanotech Research and Innovation Tower (BRIT) Laboratory of the University of Catania.

■ REFERENCES

(1) Broughton, J. P.; Deng, X.; Yu, G.; Fasching, C. L.; Servellita, V.; Singh, J.; Miao, X.; Streithorst, J. A.; Granados, A.; Sotomayor-Gonzalez, A.; Zorn, K.; Gopez, A.; Hsu, E.; Gu, W.; Miller, S.; Pan, C. Y.; Guevara, H.; Wadford, D. A.; Chen, J. S.; Chiu, C. Y. CRISPR–Cas12-based detection of SARS-CoV-2. *Nat. Biotechnol.* **2020**, *38*, 870−874.

(2) Vashist, S. K.; Luppa, P. B.; Yeo, L. Y.; Ozcan, A.; Luong, J. H. Emerging Technologies for Next-Generation Point-of-Care Testing. *Trends Biotechnol.* **2015**, *33*, 692−705.

(3) Labib, M.; Zamay, A. S.; Muharemagic, D.; Chechik, A. V.; Bell, J. C.; Berezovski, M. V. Aptamer-based Viability Impedimetric Sensor for Viruses. *Anal. Chem.* **2012**, *84*, 1813−1816.

(4) Espinosa, J. R.; Galván, M.; Quiñones, A. S.; Ayala, J. L.; Durón, S. M. DNA Biosensor Based on Double-Layer Discharge for the Detection of HPV Type 16. *Sensors* **2019**, *19*, 3956.

(5) Chowdhury, A. D.; Takemura, K.; Li, T. C.; Suzuki, T.; Park, E. Y. Electrical pulse-induced electrochemical biosensor for hepatitis E virus detection. *Nat. Commun.* **2019**, *10*, No. 3737.

(6) Ivnitski, D.; Abdel-Hamid, I.; Atanasov, P.; Wilkins, E. Biosensors for detection of pathogenic bacteria. *Biosens. Bioelectron.* **1999**, *14*, 599−624.

(7) Garibyan, L.; Avashia, N. Research Techniques Made Simple: Polymerase Chain Reaction (PCR). *J. Invest. Dermatol.* **2013**, *133*, No. e6.

(8) Son, J. H.; Cho, B.; Hong, S.; Lee, S. H.; Hoxha, O.; Haack, A. J.; Lee, L. P. Ultrafast photonic PCR. *Light Sci. App.* **2015**, *4*, e280.

(9) Zhang, J.; Song, S.; Zhang, L.; Wang, L.; Wu, H.; Pan, D.; Fan, C. Sequence-Specific Detection of Femtomolar DNA via a Chronocoulometric DNA Sensor (CDS): Effects of Nanoparticle-Mediated Amplification and Nanoscale Control of DNA Assembly at Electrodes. *J. Am. Chem. Soc.* **2006**, *128*, 8575−8580.

(10) Arugula, M. A.; Zhang, Y.; Simonian, A. L. Biosensors as 21st Century Technology for Detecting Genetically Modified Organisms in Food and Feed. *Anal. Chem.* **2014**, *86*, 119−129.

(11) Zhang, J.; Song, S.; Wang, L.; Pan, D.; Fan, C. A gold nanoparticle-based chronocoulometric DNA sensor for amplified detection of DNA. *Nat. Protoc.* **2007**, *2*, 2888.

(12) Wei, F.; Lillehoj, P. B.; Ho, C. M. DNA Diagnostics: Nanotechnology-Enhanced Electrochemical Detection of Nucleic Acids. *Pediatr. Res.* **2010**, *67*, 458−468.

(13) Gao, Z. F.; Gao, J. B.; Zhou, L. Y.; Zhang, Y.; Si, J. C.; Luo, H. Q.; Li, N. B. Rapid assembly of ssDNA on gold electrode surfaces at low pH and high salt concentration conditions. *RSC Adv.* **2013**, *3*, 12334−12340.

(14) Minaei, M. E.; Saadati, M.; Najafi, M.; Honari, H. Label-free, PCR-free DNA Hybridization Detection of Escherichia coli O157: H7 Based on Electrochemical Nanobiosensor. *Electroanalysis* **2016**, *28*, 2582−2589.

(15) Daniels, J. S.; Pourmand, N. Label-free Impedance Biosensors: Opportunities and Challenges. *Electroanalysis* **2007**, *19*, 1239−1257.

(16) Park, J. Y.; Park, S. M. DNA Hybridization Sensors Based on Electrochemical Impedance Spectroscopy as a Detection Tool. *Sensors* **2009**, *9*, 9513−9532.

(17) Le, M. H.; Jimenez, C.; Chainet, E.; Stambouli, V. A Label-Free Impedimetric DNA Sensor Based on a Nanoporous SnO_2 Film: Fabrication and Detection Performance. *Sensors* **2015**, *15*, 10686−10704.

(18) Bahadır, E. B.; Sezgintürk, M. K. A review on impedimetric biosensors. *Artif. Cells Nanomed. B.* **2016**, *44*, 248−262.

(19) Guler, Z.; Erkoc, P.; Sarac, A. S. Electrochemical impedance spectroscopic study of single-stranded DNA-immobilized electroactive polypyrrole-coated electrospun poly (ε-caprolactone) nanofibers. *Mater. Express* **2015**, *5*, 269−279.

(20) Abu-Salah, K. M.; Zourob, M. M.; Mouffouk, F.; Alrokayan, S. A.; Alaamery, M. A.; Ansari, A. A. DNA-based Nanobiosensors as an Emerging Platform for Detection of Disease. *Sensors* **2015**, *15*, 14539−14568.

(21) Rashid, J. I. A.; Yusof, N. A. The strategies of DNA immobilization and hybridization detection mechanism in the construction of electrochemical DNA sensor: A review. *Sens. Biosensing Res.* **2017**, *16*, 19−31.

(22) Lambert, M. Contagious agalactia of sheep and goats. *Revue Scientifique et Technique-Office International Des Epizooties* **1987**, *6*, 699−711.

(23) Bergonier, D.; Berthelot, X.; Poumarat, F. Contagious agalactia of small ruminants: current knowledge concerning epidemiology, diagnosis and control. *Revue Scientifique et Technique-Office International Des Epizooties* **1997**, *16*, 848−873.

(24) Loria, G. R.; Puleio, R.; Nicholas, R. A. J. Contagious Agalactia: Economic Losses and Good Practice. *J. Bacteriol. Mycol.* **2018**, *5*, 1076.

(25) Kumar, A.; Rahal, A.; Chakraborty, S.; Verma, A. K.; Dhama, K. *Mycoplasma agalactiae*, an Etiological Agent of Contagious Agalactia in Small Ruminants: a Review. *Vet. Med. Int.* **2014**, *2014*, No. 286752.

(26) Oravcová, K.; López-Enríquez, L.; Rodríguez-Lázaro, D.; Hernández, M. *Mycoplasma agalactiae* p40 Gene, a Novel Marker for Diagnosis of Contagious Agalactia in Sheep by Real-Time PCR:

Assessment of Analytical Performance and In-House Validation Using Naturally Contaminated Milk Samples. *J. Clin. Microbiol.* **2009**, *47*, 445−450.
(27) World Organization for Animal Health (OIE). Contagious agalactia. In *Manual of Diagnostic Tests and Vaccines for Terrestrial Animals (Terrestrial Manual)*; 8th ed.; OIE: Paris, 2018; Vol. *1*, https://www.oie.int/fileadmin/Home/eng/Health_standards/tahm/3.07.03_CONT_AGALACT.pdf; Chapter 3.7.3, pp 1430−1440.
(28) Jaÿ, M.; Tardy, F. Contagious Agalactia in Sheep and Goats: Current Perspectives. *Vet. Med.: Res. Rep.* **2019**, *10*, 229−247.
(29) Tumino, S.; Tolone, M.; Parco, A.; Puleio, R.; Arcoleo, G.; Manno, C.; Nicholas, R. A. J.; Loria, G. R. Validation of Loop-Mediated Isothermal Amplification (LAMP) field tool for rapid and sensitive diagnosis of Contagious Agalactia in small ruminants. *Animals* **2020**, *10*, 509.
(30) Urso, M.; Pellegrino, G.; Strano, V.; Bruno, E.; Priolo, F.; Mirabella, S. Enhanced sensitivity in non-enzymatic glucose detection by improved growth kinetics of Ni-based nanostructures. *Nanotechnology* **2018**, *29*, No. 165601.
(31) Urso, M.; Leonardi, S. G.; Neri, G.; Petralia, S.; Conoci, S.; Priolo, F.; Mirabella, S. Acetone sensing and modelling by low-cost NiO nanowalls. *Mater. Lett.* **2020**, *262*, No. 127043.
(32) Iwu, K. O.; Lombardo, A.; Sanz, R.; Scirè, S.; Mirabella, S. Facile synthesis of Ni nanofoam for flexible and low-cost non-enzymatic glucose sensing. *Sens. Actuators, B* **2016**, *224*, 764−771.
(33) Vorobyova, T. N.; Poznyak, S. K.; Rimskaya, A. A.; Vrublevskaya, O. N. Electroless gold plating from a hypophosphite-dicyanoaurate bath. *Surf. Coat. Tech.* **2004**, *176*, 327−336.
(34) Zhang, X.; Servos, M. R.; Liu, J. Instantaneous and Quantitative Functionalization of Gold Nanoparticles with Thiolated DNA Using a pH-Assisted and Surfactant-Free Route. *J. Am. Chem. Soc.* **2012**, *134*, 7266−7269.
(35) Deka, J.; Měch, R.; Ianeselli, L.; Amenitsch, H.; Cacho-Nerin, F.; Parisse, P.; Casalis, L. Surface Passivation Improves the Synthesis of Highly Stable and Specific DNA-Functionalized Gold Nanoparticles with Variable DNA Density. *ACS Appl. Mater. Interfaces* **2015**, *7*, 7033−7040.
(36) Alberts, B.; Johnson, A. D.; Lewis, J.; Morgan, D.; Raff, M.; Roberts, K.; Walter, P. *Molecular Biology of the Cell*, Vol 6; W. W. Norton & Company, 2014.
(37) Bhuvana, M.; Dharuman, V. Tethering of spherical DOTAP liposome gold nanoparticles on cysteamine monolayer for sensitive label free electrochemical detection of DNA and transfection. *Analyst* **2014**, *139*, 2467−2475.
(38) Majhi, S. M.; Naik, G. K.; Lee, H. J.; Song, H. G.; Lee, C. R.; Lee, I. H.; Yu, Y. T. Au@NiO core-shell nanoparticles as a p-type gas sensor: Novel synthesis, characterization, and their gas sensing properties with sensing mechanism. *Sens. Actuators, B* **2018**, *268*, 223−231.
(39) Muñoz, J.; Montes, R.; Baeza, M. Trends in electrochemical impedance spectroscopy involving nanocomposite transducers: Characterization, architecture surface and bio-sensing. *Trends Anal. Chem.* **2017**, *97*, 201−215.
(40) Gebala, M.; Schuhmann, W. Understanding properties of electrified interfaces as a prerequisite for label-free DNA hybridization detection. *Phys. Chem. Chem. Phys.* **2012**, *14*, 14933−14942.
(41) Rahman, M. M.; Kim, Y. J.; Lee, J. J. Label-Free Detection of DNA Hybridization by Using Charge Perturbation on Poly(thionine)-Modified Glassy Carbon and Gold Electrodes. *J. Electrochem. Soc.* **2015**, *162*, B159.
(42) Hou, L.; Cui, Y.; Xu, M.; Gao, Z.; Huang, J.; Tang, D. Graphene oxide-labeled sandwich-type impedimetric immunoassay with sensitive enhancement based on enzymatic 4-chloro-1-naphthol oxidation. *Biosens. Bioelectron.* **2013**, *47*, 149−156.
(43) Lorusso, A.; Decaro, N.; Greco, G.; Corrente, M.; Fasanella, A.; Buonavoglia, D. A real-time PCR assay for detection and quantification of *Mycoplasma agalactiae* DNA. *J. Appl. Microbiol.* **2007**, *103*, 918−923.
(44) Becker, C. A.; Ramos, F.; Sellal, E.; Moine, S.; Poumarat, F.; Tardy, F. Development of a multiplex real-time PCR for contagious agalactia diagnosis in small ruminants. *J. Microbiol. Methods* **2012**, *90*, 73−79.
(45) Vasilescu, A.; Nunes, G.; Hayat, A.; Latif, U.; Marty, J. L. Electrochemical Affinity Biosensors Based on Disposable Screen-Printed Electrodes for Detection of Food Allergens. *Sensors* **2016**, *16*, 1863.
(46) Keighley, S. D.; Li, P.; Estrela, P.; Migliorato, P. Optimization of DNA immobilization on gold electrodes for label-free detection by electrochemical impedance spectroscopy. *Biosens. Bioelectron.* **2008**, *23*, 1291−1297.

https://dx.doi.org/10.1021/acsami.0c14679
ACS Appl. Mater. Interfaces XXXX, XXX, XXX−XXX